Sequential Calcium Binding to the Regulatory Domain of Calcium Vector Protein Reveals Functional Asymmetry and a Novel Mode of Structural Rearrangement†

Isabelle Théret,‡ Sibyl Baladi,§ Jos A. Cox,§ Hiroshi Sakamoto,|| and Constantin T. Craescu*,‡

INSERM U350, Institut Curie-Recherche, Centre Universitaire, Bâtiments 110−112, 91405 Orsay, France, Département de Biochimie, Université de Genève, Suisse, and Laboratoire de Chimie Structurale des Macromolécules, Institut Pasteur, Paris, France

Received February 15, 2000; Revised Manuscript Received April 25, 2000

ABSTRACT: Calcium vector protein (CaVP) from amphioxus is a two-domain, calcium-binding protein (18.3 kDa) of the calmodulin superfamily. Only two of the four EF-hand motifs (sites III and IV) have a significant binding affinity for calcium ions. We determined the solution structure of the domain containing these active sites (C-CaVP: W81−S161), in the Ca^{2+}-saturated state, using NMR spectroscopy and restrained molecular dynamics. The tertiary structure is similar to other Ca^{2+}-binding domains containing a pair of EF-hand motifs. The apo state has spectroscopic and thermodynamic characteristics of a molten globule, with conserved secondary structure but highly fluctuating tertiary organization. Titration of C-CaVP with Ca^{2+} revealed a stepwise ion binding, with a stable equilibrium intermediate in which only site III binds a calcium ion. Despite a highly fluctuating structure of the free site IV, the calcium-bound site III has a persistent structure, with similar secondary elements but different interhelix angle and hydrophobic packing relative to the fully calcium-saturated state.

Calcium vector protein (CaVP)[1] is a unique EF-hand Ca^{2+}-binding protein of 18.3 kDa, found *in vivo* as a complex with a 26.6 kDa protein, named CaVPT (from calcium vector protein target) (*1*). Both proteins are abundant in amphioxus, a higher invertebrate which is the closest living relative of the vertebrates. Although the exact roles of CaVP and CaVPT are still unknown, the available data suggest that the bimolecular complex may regulate the invertebrate thick filament dynamics. The high sequence identity with vertebrate calmodulin (CaM) (49%) and chicken skeletal muscle troponin C (TnC) (47%) (*2*) and comparative molecular modeling (*3*) indicate that CaVP consists of two domains, each containing two potential Ca^{2+}-binding sites. However, calcium-binding isotherms showed that only two of the four sites are active (*2*). They were recently localized in the C-terminal half of the protein and designated as sites III and IV (S. Baladi and J. A. Cox, to be published). The affinities of these two sites are very different (intrinsic binding constants of 4.9×10^6 and 7.3×10^3 M^{-1}) and independent of the presence of the N-terminal domain (*4*). In the complex with CaVPT, CaVP binds Ca^{2+} ions with a strong positive cooperativity and a considerably increased (about 20-fold) affinity (*4*). The isolated C-terminal domain of CaVP is able to interact with CaVPT (S. Baladi and J. A. Cox, to be published) and can thus be considered as a regulatory domain.

As a step toward the elucidation of structure/function relationships in CaVP, we decided to determine the three-dimensional solution structure of the protein and the conformational changes induced by Ca^{2+} binding. However, CaVP showed a strong tendency to form dimers, producing broad line spectra which are detrimental to the structural analysis by NMR spectroscopy. We therefore chose to overexpress and study the N- and C-terminal domains separately. The validity of studying the isolated domains is supported by three observations: (1) the Ca^{2+}-binding constants for the C-terminal domain and the whole CaVP are the same; (2) molecular modeling of CaVP (*3*) points to the existence of a long flexible linker between the N- and C-terminal halves; (3) proteolytic as well as biochemical and functional studies on isolated domains of CaVP (J. A. Cox, data not published) provide evidence that they are structurally autonomous. In particular, the C-terminal domain could bind CaVPT in a calcium-dependent manner, but with a lower affinity. Furthermore, similar studies on isolated domains of other calcium-binding proteins, such as calmodulin (CaM) (*5*) and troponin C (TnC) (*6*−*8*), have been successfully carried out. Here we focus on the C-terminal domain of CaVP (C-CaVP) comprising residues W81−S161 (Figure 1) and report its three-dimensional solution structure in the Ca^{2+}-saturated state. In addition, we present a structural characterization of apo and $(Ca^{2+})_1$ states. As shown by calcium titration experiments, the metal ion binds in a sequential manner: first to site III, then to site IV. The stable $(Ca^{2+})_1$ intermediate species displays an unusual pairing of a well-structured ion-bound site with a fluctuating EF-hand fragment.

† This work was supported by the Centre National de la Recherche Scientifique, the Institut Curie, the Swiss National Science Foundation, and the European Community (TMR program, NMR Large Scale Facility, Utrecht).

* To whom correspondence should be addressed. Phone: 33 1 69 86 31 63. Fax: 33 1 69 07 53 27. E-mail: Gil.Craescu@curie.u-psud.fr.

‡ Institut Curie-Recherche, Centre Universitaire.

§ Université de Genève.

|| Institut Pasteur.

[1] Abbreviations: CaM, calmodulin; CaVP, calcium vector protein; C-CaVP, the C-terminal domain of CaVP (residues 81−161); CaVPT, calcium vector protein target; TnC, troponin C.

10.1021/bi000360z CCC: $19.00 © 2000 American Chemical Society
Published on Web 06/16/2000

MATERIALS AND METHODS

Sample Preparation. Cloning, expression, and purification of recombinant C-CaVP were as described previously (S. Baladi and J. A. Cox, to be published). ^{15}N-labeling was performed in a M63 medium containing appropriate antibiotics and $(^{15}NH_4)_2SO_4$ (2 g/L) as the sole source of nitrogen. The IPTG induction phase (0.1 mM final concentration) proceeded overnight. NMR samples, in the concentration range 0.8−1.3 mM, were prepared in deuterated Tris (d_{11}) buffer (20 mM), KCl (100 mM), pH 6.5, in the presence of variable $CaCl_2$ concentrations, required to obtain the apo, $(Ca^{2+})_1$, and $(Ca^{2+})_2$ states.

NMR Spectroscopy. Spectra were acquired at 308 K on a Varian Unity500 spectrometer equipped with a triple-resonance probe and Z-field gradient. Homonuclear 2D experiments used the standard pulse sequences (*9*). Heteronuclear 2D and 3D experiments were based on pulse field gradients for water suppression and coherence selection (*10*) combined with the enhanced sensitivity technique (*11*). Dihedral angle restraints were obtained by analyzing the HMQCJ spectrum according to the method proposed by Wang et al. (*12*). Spectra analysis and NOE restraints collection were carried out with Felix2.3 software (MSI, San Diego).

Structure Determination. Almost complete proton and ^{15}N resonance assignment was obtained by the analysis of homonuclear 2D and heteronuclear 3D spectra using a sequence-specific procedure (*9*). Most of the assignment was performed using proton 2D spectra. ^{1}H−^{15}N heteronuclear experiments were necessary to complete the assignment and to collect the distance restraints involving the HN groups. A table containing the ^{1}H and ^{15}N chemical shift values has been deposited in the BioMagResBank, under accession number 4739.

For the $(Ca^{2+})_2$ structure, a total number of 1004 distance restraints (including hydrogen bond restraints) were collected, representing an average of about 12 restraints per residue. NOE-derived distance restraints were classified into three categories, 1.8−2.9, 2.9−3.7, and 3.7−5.00 Å, with the exception of $d_{\alpha N}(i,i+2)$ and $d_{NN}(i,i+2)$ in regular helical fragments which fall into 4.2−4.6 and 4.0−4.4 Å, respectively. An additional 99 dihedral angular restraints, derived from vicinal coupling constants and secondary structure considerations, were included. No restraints between the calcium ions and the protein were considered explicitly. Several hydrogen bond restraints were used for the two Ca^{2+}-binding loops. One hydrogen bond is formed between the HN and a carboxylic oxygen of residues in positions 6 and 1 of the binding loop, respectively (*13*). The others correspond to typical Asx and reverse turns (*14*) generally observed in EF-hand proteins. In each case, the existence of hydrogen bond interactions was confirmed by observation of a slow exchange rate of the involved amide protons. The restraint statistics are detailed in Table 1.

The ensemble of NMR-derived distance bounds was completed using a smoothing procedure (based on triangle and tetrangle strategies) integrated in the Distance Geometry (DGII) program (MSI, San Diego). Starting from an extended conformation and using the embedding and optimization steps of DGII, we generated 100 structures which are compatible with these improved distance bounds and the chirality restraints. The best 42 structures, in terms of restraint violations, were selected and refined under a physical force field (cvff) and experimental restraints by molecular dynamics (Simulated Annealing protocol, Discover program, MSI, San Diego). The 20 final structures were retained for their low potential energy, best fit of the experimental restraints, and good covalent geometry.

Table 1: Restraint and Structural Statistics for the 20 Simulated Annealing Structures of Ca^{2+}-Saturated C-CaVP

restraint statistics	
NOE restraints	938
intraresidue	249
sequential	285
medium range ($2 < \|i-j\| < 4$)	184
long range ($\|i-j\| \geq 5$)	220
hydrogen bond restraints	66
dihedral angle restraints (Φ,Ψ)	99
average no. of NOE restraint violations	
>0.4 Å	none
>0.3 Å	1.1/structure
rmsd from exptl distance restraints (Å)	0.049 (0.002)
rmsd from exptl dihedral restraints (deg)	0.99 (0.5)
RMSD from idealized geometry	
bonds (Å)	0.0301 (0.0004)
angles (deg)	3.7 (0.4)

	av rmsd (Å) from av structure	av pairwise rmsd (Å)
secondary structure[a]	0.70 (0.09)	1.02
secondary structure[b]	1.19 (0.17)	1.73
helix 1, 2, β-strand[a]	0.53 (0.12)	0.75
helix 3, 4, β-strand[a]	0.60 (0.13)	0.86
helix 1, 2, β-strand[b]	1.12 (0.24)	1.63
helix 3, 4, β-strand[b]	1.06 (0.16)	1.54
helix 1[a]	0.31 (0.12)	
helix 2[a]	0.21 (0.07)	
helix 3[a]	0.25 (0.05)	
helix 4[a]	0.31 (0.12)	
(Φ,Ψ) in most-favored region	83.2%	

[a] Backbone atoms (N, C′, Cα). [b] All heavy atoms.

Coordinates. The 20 best structures and the energy-minimized average structure of the $(Ca^{2+})_2$ form have been deposited in the Protein Data Bank under accession codes 1C7V and 1C7W, respectively.

RESULTS AND DISCUSSION

Structure of C-CaVP in the Ca^{2+}-Saturated State. The NMR spectra of the fully saturated C-CaVP were recorded in the presence of 5 mM $CaCl_2$. Secondary structure elements were first identified from the combined analysis of short- and medium-range NOE connectivities, the chemical shift index of Hα protons, coupling constants ($^3J_{HNH\alpha}$), and amide proton exchange rates. Four α-helices (E−H) were thus defined within the following limits: E87−F97, F107−Q115, D124−A134, and I144−K152 (Figure 1). Two β-strands were also identified (V104−D106 and V141−D143) by the low-field-shifted Hα protons, strong $d_{\alpha N}(i,i+1)$ sequential connectivities, large $^3J_{HNH\alpha}$ couplings, and a highly reduced exchange rate of amide protons. Typical strong dipolar interactions between Hα protons on opposite strands (Hα106/Hα141; Hα104/Hα143) enabled us to establish the topology

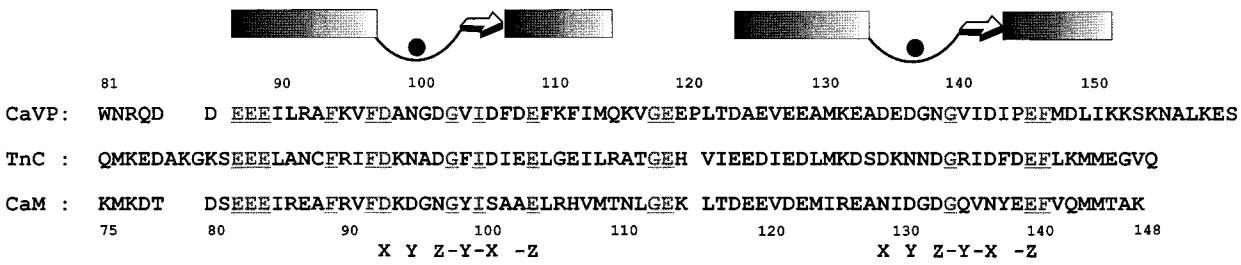

FIGURE 1: Sequence comparison between the C-CaVP, studied in this work, and the C-terminal domains of CaM and TnC. Residues conserved in the three sequences are in gray and underlined. The secondary structure elements observed in C-CaVP and the Ca^{2+} ligands in calcium loops are shown on the top and the bottom of the alignment, respectively.

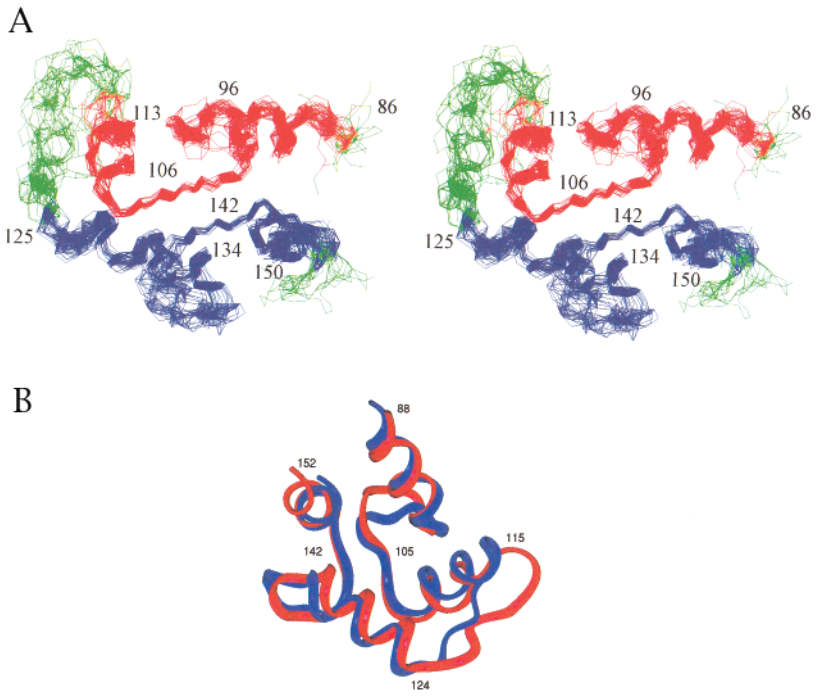

FIGURE 2: Three-dimensional structure of the Ca^{2+}-saturated C-CaVP. (a) Stereo representation of the best superposition of the 20 final structures, refined under the NMR restraints. Shown are backbone atoms (N, C′, Cα) in residues 86−154. The EF-hand motifs III and IV are colored in red and blue, respectively. (b) Structure comparison of Ca^{2+}-saturated C-CaVP (red) and the C-terminal domain of CaM (blue). Best superposition of the backbone heavy atoms in corresponding regular secondary structure elements. C-CaVP is represented by the energy-minimized average NMR structure, while CaM is represented by the crystallographic structure (pdb code 3cln).

of the small two-stranded antiparallel β-sheet. The observed secondary structure elements are identical (within ±1 residue) to those of the C-terminal domains of CaM or TnC.

Superposition of the backbones of 20 energy-refined final structures is shown in a stereo representation in Figure 2a. The four α-helices (E−H) form two EF-hand motifs, connected by the two-stranded antiparallel β-sheet. The N- and C-termini as well as the loop linking the two binding sites are less defined due to a smaller number of NOE data. The structure is highly similar to the EF-hand pair commonly observed in the CaM superfamily. Several criteria were employed to evaluate the precision and quality of the determined structures: agreement with the experimental restraints, deviation from idealized geometry (bond length, bond angle, Cα chirality, peptide bond planarity), distribution of the (Φ, Ψ) angles in the Ramachandran plot, and the superposition of the final structures (Table 1). The majority of the residues fall in the favorable bi-dimensional regions of the (Φ, Ψ) space (83%), with about 1% in disallowed regions. When compared separately, the helices and strands are very well-defined (Table 1), with rms distance values on the order of 0.27 Å. The increased rms distance for the whole structure results from the higher uncertainty in the relative orientation of the four helices. This analysis allowed the 20 energy-refined structures to be considered an accurate representation of the solution structure of C-CaVP. The quality of the structure is comparable to other solution structures of EF-hand domains (*5*, *6*, *8*).

The values of interhelical angles within an EF-hand, determined for the 20 refined structures of C-CaVP, are 116 ± 5° and 90 ± 7° for sites III and IV, respectively. The angle value observed for EF-hand IV in C-CaVP is very close to the average value observed in the bound regulatory domains, i.e., 95 ± 9° (*15*), while the site III angle is significantly larger. In general, the interhelical angles in regulatory Ca^{2+}-binding domains, e.g., the N-terminal domain of TnC or recoverin, both N- and C-terminal domains of CaM, are significantly smaller in the ion-bound state than in the apo state, yielding a more open tertiary structure, with exposed hydrophobic patches (*8*). Similarly to other Ca^{2+} sensors, ion-bound C-CaVP has an extensive, well-packed hydrophobic core including 4 Phe, 6 Ile, 1 Leu, 1 Val, and

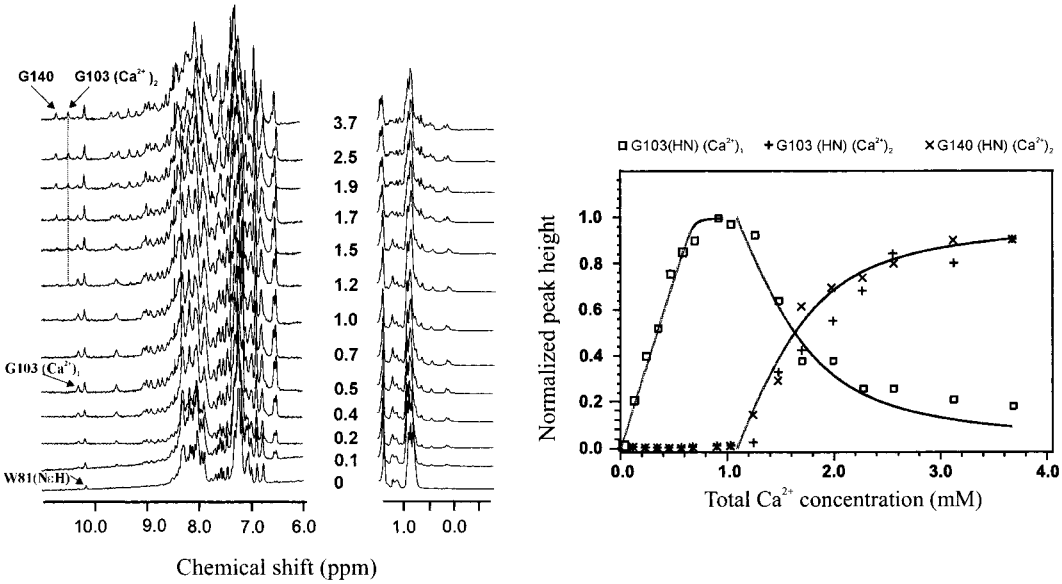

FIGURE 3: Ca^{2+} titration of 1 mM C-CaVP in Tris-HCl buffer (pH 6.5) containing 100 mM KCl, at 308 K. Left: 1D NMR spectral regions corresponding to aromatic/amide protons and to ring current-shifted aliphatic protons are shown as a function of the total Ca^{2+} concentration in solution (middle column, in mM). Right: graphical representation of the Ca^{2+}-dependent normalized, dilution-corrected peak intensity for the amide proton of G103 in the $(Ca^{2+})_1$ species and for amide protons of G103 and G140 in the $(Ca^{2+})_2$ species. The continuous curves represent the theoretical populations of one-ion and two-ion species, calculated for two independent binding processes with association constants of 5×10^6 and 3.3×10^3 M^{-1} for the first and second step, respectively.

3 Met residues. The calculated apolar accessible surface represents 60% of the total accessible surface, which is slightly larger than in the homologous Ca^{2+}-saturated domains of CaM (52%) and TnC (57%).

Superposition of the energy-minimized average structure of C-CaVP on the crystal structures of the C-terminal domains of either CaM (pdb code 3cln) (Figure 2b) or TnC (pdb code 1ncx), using the best fit of the backbone atoms (N, C′, Cα) in regular segments, resulted in an rms distance of 2.0 Å in both cases. Fitting of individual EF-hand motifs is significantly better (rms distances of about 0.9 and 1.4 Å for sites III and IV, respectively), indicating that a large part of the difference in tertiary structure arises from the relative position of the motifs in each domain. As the loop connecting the two EF-hands is usually flexible, the presence of a Pro insert (Pro121) in the corresponding sequence (Figure 1) may hardly be invoked to explain the observed packing of the four helices. The specific tertiary fold is rather determined by specific intramolecular interactions between the side chains forming the hydrophobic core.

The Ca^{2+}-Free Protein Is in a Disordered State. The far-UV circular dichroism (CD) spectrum of apo C-CaVP is indicative of the presence of α-helical structure, but, according to the molar ellipticity at 222 nm, its content (about 17%) is about 2-fold lower than in the calcium-saturated state (36%) (data not shown). Temperature denaturation, monitored by CD spectropolarimetry, showed that the secondary structure elements in the ion-free C-CaVP unfold in a cooperative manner, with a mid-temperature of 55 °C, i.e., at least 35 °C below that of the fully Ca^{2+}-saturated protein. Thermodynamic analysis of the experimental data (*16*) yielded an enthalpy change for unfolding at 55 °C of about 40 kcal/mol, a value which is characteristic for low-stability structures. However, observation of a cooperative transition suggests that the weak tertiary interactions are still able to maintain a relatively compact structure.

The 1D and 2D NMR spectra of the apo form are characteristic of a highly flexible polypeptide conformation with no, or a very fluctuating, tertiary structure, reflected in the poor dispersion of the proton resonances, which are closer to the random coil values than to the native $(Ca^{2+})_2$ state values. For instance, the amide protons resonate between 7.7 and 8.6 ppm, the Cα protons are found between 3.8 and 4.7 ppm, and the methyl groups give a large, unresolved peak centered at ~0.9 ppm (Figure 3). Moreover, the spectra are not significantly modified by changes in ionic strength from 0.0 to 0.2 M. The NMR data provide direct evidence for the absence of persistent hydrogen bond interactions, the lack of persistent tertiary contacts involving aromatic side chains, and the absence of β-type backbone conformation (no low-field-shifted Cα protons).

Taken together, these observations suggest that the apo state is a dynamic equilibrium of multiple, relatively compact conformations, having a decreased helical content relative to the $(Ca^{2+})_2$ state. We hypothesize that the helical fragments slide rapidly up and down along the sequence with fast kinetics and are thus undetectable by NMR spectroscopy. Therefore, the metal-free species exhibits many characteristics of proteins in a molten globule state (*17*).

Sequential Ca^{2+} Binding. Within the Ca^{2+} sensor subfamily, metal binding induces significant conformational changes, which trigger the interaction with the target molecule. To better characterize the ion-binding process and its structural consequences in C-CaVP, we performed a Ca^{2+} titration experiment and analyzed in more detail the main intermediate state on the pathway of $(Ca^{2+})_2$ complex formation. Figure 3 (left) shows a series of 1D NMR spectra of C-CaVP (1 mM) in the presence of increasing Ca^{2+} concentrations, from 0 to 3.7 mM. Both low-field (aromatic and amide) and upfield (aliphatic) spectral regions evolve from a compact, low-dispersion form in the apo state, toward a well-dispersed spectrum, characteristic of native proteins. A qualitative

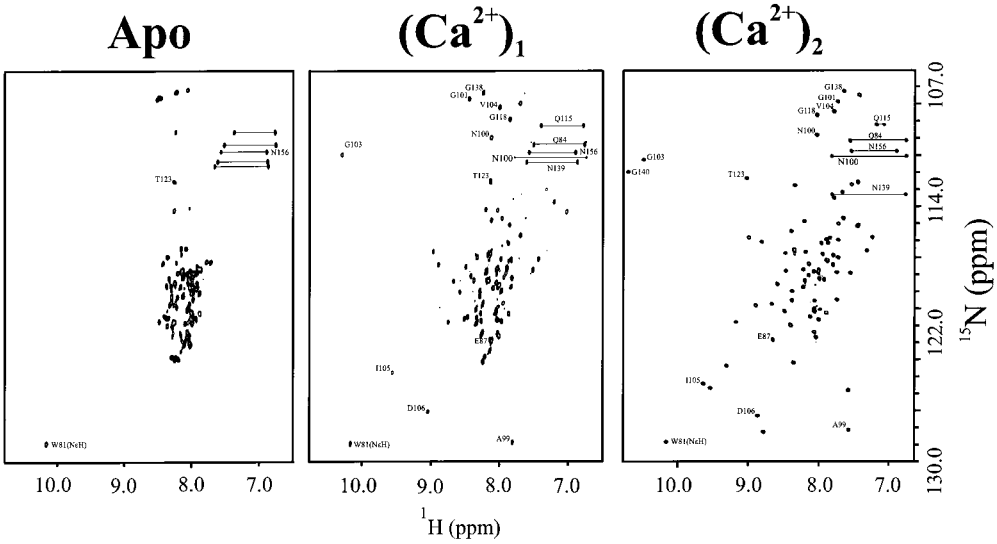

FIGURE 4: ($^{15}N-^{1}H$)-HSQC spectra of C-CaVP in the apo, $(Ca^{2+})_1$, and $(Ca^{2+})_2$ states. Samples (1 mM) were in deuterated Tris-DCl buffer containing 100 mM KCl, pH 6.5, at 308 K. $CaCl_2$ concentration was 0, 1, and 5 mM in apo, $(Ca^{2+})_1$, and $(Ca^{2+})_2$ samples, respectively. Horizontal lines connect pairs of cross-peaks from Gln and Asn side chains. Some of the assigned cross-peaks are indicated by the type and number of the residue.

analysis of the successive spectra revealed two distinct steps, corresponding to sequential binding of two calcium ions. During the two transitions, the peaks of the emerging species have a constant chemical shift and an increasing intensity, suggesting a slow exchange regime on the chemical shift scale. The three binding states [apo, $(Ca^{2+})_1$, and $(Ca^{2+})_2$] have distinct spectral features and are stable enough to be studied independently. Along the titration experiment, the spectral line width shows no significant broadening, suggesting that changes in metal occupancy are not accompanied by a perceptible aggregation.

A more quantitative evaluation of the binding process is presented in Figure 3 (right), where the normalized intensity of some resolved peaks is plotted as a function of the total metal ion concentration. Theoretical curves, calculated for two successive, independent bi-molecular processes (*18*) with association constants of 5×10^6 and 3.3×10^3 M^{-1}, appear to simulate satisfactorily the experimental data. This NMR titration experiment is certainly not appropriate for an accurate determination of the binding constants, but we note that the above values are in good agreement with those determined by flow dialysis (*4*).

A global view of the spectral changes caused by Ca^{2+} binding may be obtained from the analysis of ($^{1}H-^{15}N$)-HSQC spectra of the apo, $(Ca^{2+})_1$, and $(Ca^{2+})_2$ states (Figure 4). The line widths of the observed cross-peaks are similar in the three spectra, which suggests no molecular association and a slow exchange regime for all the peaks. This last conclusion is supported by NOESY spectra acquired during the titration (with a mixing time of 200 ms) which showed no exchange cross-peaks between resonances representing the same residue in different ligation states. Binding of the first Ca^{2+} affects only one subensemble of peaks, whereas binding of the second Ca^{2+} perturbs nearly the whole spectrum, suggesting that the first Ca^{2+} organizes only its binding site, while the second ion modifies the entire domain (Figure 4). The sequential binding, described here for C-CaVP, is different from the stepwise process observed for the regulatory domain of TnC (*19*), in which binding of each Ca^{2+} ion induces changes throughout the whole domain and the higher affinity site is not clearly assigned. This difference should be mainly related to the large difference in Ca^{2+} affinity between the two binding sites of C-CaVP.

The First Ca^{2+} Ion Is Bound to Site III. NMR spectra of the $(Ca^{2+})_1$ species show a chemical shift dispersion which is intermediate between the apo and $(Ca^{2+})_2$ forms (Figures 3 and 4). A closer inspection of the HSQC spectra (Figure 4) revealed that only half of the resonances exhibit large chemical shift changes (up to 2 ppm) upon addition of the first metal ion, while the other resonances are practically unchanged.

Analysis of several 2D and 3D ($^{1}H-^{15}N$) NMR experiments, acquired in the presence of an equimolar concentration of Ca^{2+}, enabled us to assign unambiguously resonances corresponding to a continuous string of 34 residues from D85 to G118, representing the binding site III. The chemical shift values for these residues are similar, but not identical, to those observed in the $(Ca^{2+})_2$ form, suggesting the existence of structural differences between the two bound forms. In contrast, the residues lying outside this segment give poorly dispersed resonances, which were difficult to assign unambiguously. These observations indicate that the first Ca^{2+} ion is bound to the EF-hand III, which adopts a stable and regular structure, while the rest of the sequence remains highly fluctuating. Spectral analysis allowed us to set up a restraint file of 341 distance, hydrogen bond, and angular restraints for the fragment D85−G118, covering the first Ca^{2+}-bound EF-hand motif. This represents a reasonable number of structural data for the folded fragment (on average, 10 restraints per residue), enabling us to determine the fragment structure. Using the experimental data and the distance geometry/simulating annealing procedure, we calculated 18 structures representing segment 85−118 in the $(Ca^{2+})_1$ state. Their analysis, according to several criteria (residual restraint violations, rms distances, deviations from idealized covalent geometry, (Φ, Ψ) distribution, etc.), attests that the structures are of good quality and well-defined (Table 2). Despite the fluctuating character of the ion-free half, binding site III is folded as a common EF-hand motif, including a short extended segment (V104−D106) with the same spectral and

Table 2: Restraint and Structural Statistics for the 18 Simulated Annealing Structures of Ca^{2+}-Bound EF-Hand III (D85−G118) in C-CaVP

restraint statistics	
NOE restraints	273
intraresidue	62
sequential	102
medium range ($2 < \|i - j\| < 4$)	62
long range ($\|i - j\| \geq 5$)	47
hydrogen bond restraints	26
dihedral angle restraints (Φ,Ψ)	42
av no. of NOE restraint violations	
>0.4 Å	none
>0.3 Å	0.55/structure
rmsd from exptl distance restraints (Å)	0.071 (0.007)
rmsd from exptl dihedral restraints (deg)	2.3 (0.4)
rmsd from idealized geometry	
bonds (Å)	0.031 (0.001)
angles (deg)	3.7 (0.3)

	av rmsd (Å) from av structure	av pairwise rmsd (Å)
residus 90−115[a]	0.55 (0.13)	0.80 (0.09)
residus 90−115[b]	1.53 (0.14)	
helix 1[a]	0.24 (0.05)	
helix 2[a]	0.30 (0.11)	
(Φ,Ψ) in most-favored region	73.5%	

[a] Backbone atoms (N, C′, Cα). [b] All atoms.

conformational features as in an antiparallel β-sheet. The two α-helices (I90−F97, F107−M114) define an interhelix angle of 82 ± 9°, i.e., more than 30° smaller than in the $(Ca^{2+})_2$ state (Figure 5). A large part of this conformational change is due to a rotation of the E helix around a small hinge, situated at the end of the helix, similarly to the open/closed movement observed in CaM and TnC (*20*). In the absence of a hydrophobic contribution from the second motif, an intra-motif hydrophobic cluster is built around a scaffold involving F94, F107, and F110. As illustrated in Figure 5, the three Phe residues are far away from each other in the $(Ca^{2+})_2$ state, where their clustering is prohibited by the presence of site IV hydrophobic side chains, like M131, I142, and F147. In the $(Ca^{2+})_1/(Ca^{2+})_2$ transition, F107 and F110 undergo only small rearrangements, mainly side chain rotations, whereas F94 moves away from F107 and F110 by more than 4 Å, to interact with F147. It may be reasonably assumed that this hydrophobic cluster formation plays an important role in triggering the E helix rotation and the formation of the tertiary structure in the $(Ca^{2+})_2$ state during the transition from $(Ca^{2+})_1$ to the $(Ca^{2+})_2$ form.

Nuclear relaxation measurements on ^{15}N nuclei in C-CaVP provide interesting information on the different internal dynamics of the two Ca^{2+}-bound forms. Heteronuclear steady-state NOEs (η) between proton and nitrogen nuclei in amide groups were obtained by recording spectra with and without proton saturation before the start of the experiment (*10*). The site III segment, which is well structured in the partial Ca^{2+}-bound form, has similar η values (around −0.3) and sequence dependence as in the fully Ca^{2+}-saturated form. In contrast, the rest of the chain in $(Ca^{2+})_1$ state gives scattered NOE values ranging from −0.5 to −1.5, which are characteristic for loosely packed, fluctuating, but not completely unfolded structures (*21*, *22*).

Biological Implications. Apo C-CaVP represents a new example of a protein which, under nondenaturant conditions, is in a loosely packed, disordered state, sharing many characteristics with the molten globule state (*17*). An increasing number of examples of native unfolded or structurally disordered proteins under normal solution conditions have been described in the past few years (*22*−*29*). Their functional significance is not well understood, but in some cases the disordered state was invoked to explain the transport through narrow channels (*22*) or to provide enough conformational flexibility necessary in molecular recognition and/or assembly formation (*26*, *29*). Even if the functional role of C-CaVP remains to be discovered, the metal-induced disorder-to-order transition represents a good working model for investigation of structural and thermodynamic aspects of protein folding.

The Ca^{2+}-dependent conformational features observed in C-CaVP have no similar counterpart in any other EF-hand proteins studied so far. Generally, proteins of this family show a well-folded and persistent structure in the absence of metal and undergo a helix rearrangement upon Ca^{2+} binding. For calbindin D_{9k} (a Ca^{2+} buffer), for instance, the rms distance between apo and $(Ca^{2+})_2$ is 1.23 Å (*30*), while for the C-terminal domain of CaM (a Ca^{2+} sensor) the rms distance is about 4.5 Å (*5*).

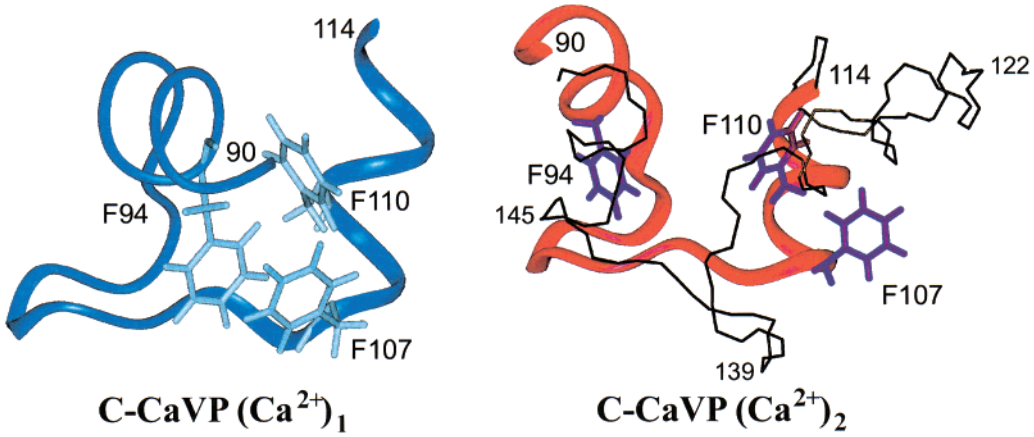

FIGURE 5: Ribbon structure of the Ca^{2+}-bound EF-hand III motif in the $(Ca^{2+})_1$ and $(Ca^{2+})_2$ states. Three side chains from the hydrophobic core are explicitly shown in a stick representation in the two cases. The main-chain trace of the EF-hand IV is shown in black for the Ca^{2+}-saturated form. The figure was prepared using Insight software.

In contrast with C-CaVP, the NMR spectra of Ca^{2+}-free CaM or TnC are well-dispersed, allowing resonance assignment and solution structure determination to be performed (*8*, *31*). However, in the case of CaM, the apo form of the C-terminal domain shows some dynamic disorder due to a global conformational exchange in the microsecond to millisecond time scale and to a rapid conformational averaging of the side chains in the protein core (*32* − *34*).

The present ion-induced structural changes in C-CaVP define an original behavior within the EF-hand repertoire. The sequential calcium binding induces a progressive, stepwise transition from a highly disordered protein state into a half-structured conformation and finally into a standard EF-hand pair. Analysis of Ca^{2+} titration experiments using CaVP indicated that the C-terminal domain has a similar metal-dependent behavior when it is linked to the N-terminal domain, within the intact protein (I. Théret and C. T. Craescu, unpublished results). Therefore, the present observations on the isolated domain could be confidently extrapolated to the intact protein and may have a physiological significance. The Ca^{2+}-induced structural and dynamic changes of C-CaVP represent a new mode of structural transition with a highly asymmetric intermediate.

The low Ca^{2+} affinity of site IV in C-CaVP may be related to the absence of an acidic side chain in the chelating position Z (Asn139) of the calcium loop (*35*) and probably to a lower overall hydrophobicity of the α-helices (*36*, *37*), particularly of helix G. The Pro residue at position 11 of the Ca^{2+} loop IV may be tolerated with only minor functional perturbations, as it is within site II of CaM.

As the Ca^{2+} binding to CaVP was not modified by the presence of 2 mM Mg^{2+}, it was concluded that the two binding sites are Ca^{2+}-specific (*4*). Therefore, it is reasonable to assume that under resting conditions (i.e., no Ca^{2+} signal) the free protein is merely in the apo form, and that a small increase in free [Ca^{2+}] leads to the $(Ca^{2+})_1$ state, characterized by a well-folded site III and a large flexibility of site IV. The complex formed by CaVP/CaVPT binds equally two Ca^{2+} ions but with a larger affinity and a positive cooperativity (*4*). We may reasonably conceive that the folded EF-hand III is the physiological trigger, which, in the presence of the natural target CaVPT, induces structure in the EF-hand IV and subsequent Ca^{2+} binding to this otherwise unphysiologically low-affinity site. The dramatically increased calcium affinity of the CaVP/CaVPT complex, as compared to isolated CaVP (*4*), could be explained by a structural stabilization of site IV, induced by complex formation.

ACKNOWLEDGMENT

We thank Lewis E. Kay for providing pulse sequences and Gary Gippert for the GAP software.

REFERENCES

1. Cox, J. A. (1986) *J. Biol. Chem. 261*, 13173−13178.
2. Kobayashi, T., Takagi, T., Konishi, K., and Cox, J. A. (1987) *J. Mol. Biol. 262*, 2613−2623.
3. Cox, J. A., Alard, P., and Schaad, O. (1990) *Protein Eng. 4*, 23−32.
4. Petrova, T. V., Comte, M., Takagi, T., and Cox, J. A. (1995) *Biochemistry 34*, 312−318.
5. Finn, B. E., Evenäs, J., Drakenberg, T., Waltho, J. P., Thulin, E., and Forsén, S. (1995) *Nat. Struct. Biol. 2*, 777−783.
6. Slupsky, C. M., and Sykes, B. D. (1995) *Biochemistry 34*, 15953−15964.
7. Spyracopoulos, L., Li, M. X., Sia, S. K., Gagné, S. M., Chandra, M., Solaro, R. J., and Sykes, B. D. (1997) *Biochemistry 36*, 12138−12146.
8. Gagné, S. M., Tsuda, S., Li, M. X., Smillie, L. B., and Sykes, B. D. (1995) *Nat. Struct. Biol. 2*, 784−789.
9. Wüthrich, K. (1986) *NMR of proteins and nucleic acids*, Wiley, New York.
10. Farrow, N. A., Muhandiram, R., Singer, A. U., Pascal, S. M., Kay, C. M., Gish, G., Shoelson, S. E., Pawson, T., Forman-Kay, J. D., and Kay, L. E. (1994) *Biochemistry 33*, 5984−6003.
11. Cavanagh, J., Palmer, A. G., III, Wright, P E., and Rance, M. (1991) *J. Magn. Reson. 91*, 429−436.
12. Wang, Y., Nip, A. M., and Wishart, D. S. (1997) *J. Biomol. NMR 10*, 373−382.
13. Krudy, G. A., Brito, R. M. M., Putkey, J. A., and Rosevear, P. R. (1992) *Biochemistry 31*, 1595−1602.
14. Herzberg, O., and James, M. N. G. (1985) *Biochemistry 24*, 5298−5302.
15. Gagné, S. M., Li, M. X., and Sykes, B. D. (1997) *Biochemistry 36*, 4386-4392.
16. Pace, C. N., Shirley, B. A., and Thomson, J. A. (1989) in *Protein structure: a practical approach* (Creighton, T. E., Ed.) pp 311−330, IRL Press, Oxford.
17. Ptitsyn, O. B. (1995) *Curr. Opin. Struct. Biol. 5*, 74−78.
18. Lian, L. Y., Barsukov, I. L., Sutcliffe, M. J., Sze, K. H., and Roberts, G. C. K. (1994) *Methods Enzymol. 239*, 657−700.
19. Li, M. X., Gagné, S. M., Tsuda, S., Kay, C. M., Smillie, L. B., and Sykes, B. D. (1995) *Biochemistry 34*, 8330−8340.
20. Houdusse, A., Love, M. L., Dominguez, R., Grabarek, Z., and Cohen, C. (1997) *Structure 5*, 1695−1711.
21. Alexandrescu, A. T., and Shortle, D. *J.* (1994) *J. Mol. Biol. 242*, 527−546.
22. Daughdrill, G. W., Chadsey, M. S., Karlinsey, J. E., Hughes, K. T., and Dahlquist, F. W. (1997) *Nat. Struct. Biol. 4*, 285−291.
23. Gast, K., Damaschun, H., Eckert, K., Schulze-Forster, K., Maurer, H. R., Müller-Frohne, M., Zirwer, D., Czarnecki, J., and Damaschun, G. (1995) *Biochemistry 34*, 13211−13218.
24. Prêcheur, B., Cox, J. A., Petrova, T., Mispelter, J., and Craescu, C. T. (1996) *FEBS Lett. 395*, 89−94.
25. Weinreb, P. H., Zhen, W., Poon, A. W., Conway, K. A., and Lansbury, P. T., Jr. (1996) *Biochemistry 35*, 13709−13715.
26. Kriwacki, R. W., Hengst, L., Tennant, L., Reed, S. I., and Wright, P. E. (1996) *Proc. Natl. Acad. Sci. U.S.A. 93*, 11504−11509.
27. Josefsson, E., O'Connel, D., Foster, T. J., Durussel, I., and Cox, J. A. (1998) *J. Biol. Chem. 273*, 31145−31152.
28. Mok, Y.-K., Kay, C. M., Kay, L. E., and Forman-Kay, J. (1999) *J. Mol. Biol. 289*, 619−638.
29. Lydakis-Simantiris, N., Hutchison, R. S., Betts, S. D., Barry, B. A., and Yocum, C. F. (1999) *Biochemistry 38*, 404−414.
30. Skelton, N. J., Kördel, J., and Chazin, W. J. (1995) *J. Mol. Biol. 249*, 441−462.
31. Kuboniwa, H., Tjandra, N., Grzesiek, S., Ren, H., Klee, C. B., and Bax, A. (1995) *Nat. Struct. Biol. 2*, 768−776.
32. Tjandra, N., Kuboniwa, H., Ren, H., and Bax, A. (1995) *Eur. J. Biochem. 230*, 1014−1024.
33. Zhang, M., Tanaka, T., and Ikura, M. (1995) *Nat. Struct. Biol. 2*, 758−767.
34. Urbauer, J. L., Short, J. H., Dow, L. K., and Wand, A. J. (1995) *Biochemistry 34*, 8099−8109.
35. Reid, R. E. (1990) *J. Biol. Chem. 265*, 5971−5976.
36. Sekharudu, Y. C., and Sundaralingam, M. (1988) *Protein Eng. 2*, 139−146.
37. Wang, S., George, S. E., Davis, J. P., and Johnson, J. D. (1998) *Biochemistry 37*, 14539−14544.

BI000360Z